Long-range order and quantum criticality in antiferromagnetic chains with long-range staggered interactions

Jie Ren, Zhao Wang, and Weixia Chen
Department of Physics, Changshu Institute of Technology, Changshu 215500, China

Wen-Long You*
College of Science, Nanjing University of Aeronautics and Astronautics, Nanjing, 211106, China
and MIIT Key Laboratory of Aerospace Information Materials and Physics,
Nanjing University of Aeronautics and Astronautics, Nanjing 211106, China

(Received 7 September 2021; accepted 4 March 2022; published 21 March 2022)

We study quantum phase transitions in Heisenberg antiferromagnetic chains with a staggered power-law decaying long-range interactions. Employing the density-matrix renormalization group (DMRG) algorithm and the fidelity susceptibility as the criticality measure, we establish more accurate values of quantum critical points than the results obtained from the spin-wave approximation, quantum Monte Carlo, and DMRG in literatures. The deviation is especially evident for strong long-range interactions. We extend isotropic long-range interactions to the anisotropic cases and find that kaleidoscope of quantum phases emerge from the interplay of anisotropy of the long-range exchange interaction and symmetry breaking. We demonstrate nonfrustrating long-range interactions induce the true long-range order in Heisenberg antiferromagnetic chains with a continuous symmetry breaking, lifting the restrictions imposed by the Mermin-Wagner theorem.

DOI: 10.1103/PhysRevE.105.034128

I. INTRODUCTION

As a prototypical model of magnetism, antiferromagnetic (AFM) Heisenberg model $H = \sum_{i,j} J_{i,j} \vec{S}_i \cdot \vec{S}_j$ has been persistently investigated for decades [1]. Despite being a simplified theoretical model, the Heisenberg model finds applications in a variety of contexts, ranging from quantum phase transitions (QPTs) [2–6], superconductivity [7], localization in disordered systems [8], spin liquid [9], quantum chaos [10], to quantum information [11]. The ground state of the nearest-neighbor AFM Heisenberg model on a bipartite lattice in d ($\geqslant 2$) dimensions is generally expected to host Néel long-range order (LRO) for any spin magnitude S, although a rigorous proof of the existence of LRO in a two-dimensional quantum-spin-1/2 Heisenberg magnet is still lacking [12–14]. It was recognized that imposed by the Mermin-Wagner theorem, the true LRO is prohibited in short-range interacting Heisenberg model in one spatial dimension. Pioneering work by Haldane demonstrated that Heisenberg AFM chains of integer spins are endowed with a symmetry-protected topological gapped ground state [15,16], in stark contrast to the well-known spin-1/2 analog, which supports a quasi-long-range ordered critical phase, known as the Tomonaga-Luttinger liquid (TLL). In this regard, higher-dimensional magnets provide a testbed for spin-wave theory, while the spin-wave approximation usually fails in one dimension. The remarkable difference between one-dimensional (1D) AFM systems of integer and half-integer spins opens a highly successful avenue in understanding the low-dimensional strongly correlated electronic materials. The isotropic Heisenberg AFM model has been unexpectedly coined in a number of nearly ideal quasi-one-dimensional materials such as $Cu(C_4H_4N_2)(NO_3)_2$ [17], $Sr_2Cu(PO_4)_2$ [18], $KCuF_3$ [19], $CuSO_4\,5D_2O$ [20], and spin-1 chain materials like $SrNi_2V_2O_8$ [21,22], $Ni(C_2H_8N_2)_2NO_2(ClO_4)$ [23,24], and NiI_2 $(C_7H_9N)_4$ [25]. There have also been attempts to realize spontaneous symmetry breaking and develop true AFM order in spin-1/2 Heisenberg chains. One scheme under the consideration is the inclusion of the long-range interactions [26], which effectively increases the dimensionality and lifts the rigorous restrictions imposed by the Mermin-Wagner theorem.

In fact, long-range interactions occur naturally in numerous quantum materials [27–30] and versatile quantum simulators [31–34]. Especially it has been suggested that the existing cavity-mediated cold atom system [35] or Rydberg dressed atoms [36–39] could be more ideal experimental platforms for long-range interactions than solid-state ones. For instance, the interacting radius of the effective interaction between dressed atoms and the potential shape can be finely tuned by dressing to different fine-structure split states [40–43]. The typical models have considered interactions decaying with distance r as a power law $\propto 1/r^{\alpha}$ or a staggered power law $\propto (-1)^r/r^{\alpha}$, ranging from dipolar spin chain [44], Haldane-Shastry chain [45], to spin-1 chain [46,47]. The effective exchange interactions mediated by either photons or Rydberg dressing are generally U(1) or $\mathbb{Z}_2$-symmetric, and a high degree of symmetry, ideally SU(2), can be achieved by adjusting the laser detunings or increasing bosonic modes. To be specific, it is

*wlyou@nuaa.edu.cn

found that the long-range interactions of the longitudinal component results in a Wigner crystal phase [48,49], whereas the transversal one may break a continuous symmetry, resulting in a continuous symmetry-breaking phase [49,50].

Inspired by the rapid development of quantum information science, various information measurements have been exploited to study of quantum critical phenomena in spin chains. The well-known and widely studied measures are entanglement entropy (EE) [51,52] and fidelity susceptibility (FS), which diverges at the critical points in the thermodynamic limit [53,54]. The ground-state EE and FS were deemed to be capable of qualifying QPTs in many-body systems with short-range interactions [55–61], even for long-range interacting system [62–64]. In the paper, we will detect the phase transitions in AFM Heisenberg chain with long-range anisotropic interactions by the FS and the EE.

The remainder of this paper is organized as follows. We introduce the $S = 1/2$ Heisenberg model with long-range anisotropic interactions in Sec. II. The details of numerical methods and measurements are also introduced. In Sec. III, effects of long-range interactions on correlation functions, the FS and the EE are investigated. The discussion and summary are presented in the last section.

II. HAMILTONIAN AND MEASUREMENTS

In what follows, we are interested in a 1D spin-1/2 nearest-neighbor isotropic AFM chain under the effect of anisotropic long-range Heisenberg anisotropic interactions, given by

$$H = J\sum_i \Bigg\{ \vec{S}_i \cdot \vec{S}_{i+1} - \sum_{r\geqslant 2} \lambda_{i,i+r} \big[\Delta^{xy} \big(S_i^x S_{i+r}^x + S_i^y S_{i+r}^y \big) + S_i^z S_{i+r}^z \big] \Bigg\}, \tag{1}$$

where S_i^β ($\beta = x, y, z$) are spin-1/2 operators at ith site among total L sites. The AFM coupling $J = 1$ between the nearest-neighbor spins is set up as an energy unit for simplicity unless otherwise stated. The connectivity between two spins at sites i and $i + r$ separated by a distance of $r(\geqslant 2)$ is given by

$$\lambda_{i,i+r} \equiv \lambda(-1)^r r^{-\alpha}, \tag{2}$$

for the nonfrustrating long-range interactions. Here we always choose the nearest-neighbor interactions to be isotropic, favoring a TLL ground state. The deformation of beyond-nearest-neighbor couplings breaking from SU(2) symmetry down to a U(1) symmetry is characterized by the anisotropy parameter Δ^{xy} within the x-y plane, which recovers isotropic interactions for $\Delta^{xy} = 1$ and reduces to $\mathbb{Z}_2$-symmetric Ising interactions for $\Delta^{xy} = 0$. In this vein, the interplay of nearest-neighbor isotropic and longer-range anisotropic interactions admits certain magnetic symmetry breaking and stabilizes kaleidoscope of quantum phases. While a solid-state implementation of Hamiltonian Eq. (1) remains challenging, engineering such graph of interactions can be possibly realized in state-of-the-art cavity QED [65]. To be explicit, in an array of atomic ensembles within an optical cavity, the strength of spin-spin interaction patterns, including the flip-flop and diagonal interactions as well as the decay exponent, can be delicately resolved in a multimode cavity QED with an additional drive field [66], and the changing sign is determined by the phase of the corresponding sinusoidal modulation [67]. The unprecedented controllability of the cavity QED highlight the graph of interactions in Hamiltonian Eq. (1) becomes programmable.

The simultaneous appearance of long-range interactions and symmetry breaking leads to quantum critical phenomena that is different from short-range interactions. In the limit of $\alpha \to \infty$ or $\lambda \to 0$, the Hamiltonian in Eq. (1) is reduced to a spin-1/2 chain solely with the nearest-neighbor interactions, which can be analytically solved by Bethe ansatz [68]. For generic parameters $\{\alpha, \lambda\}$, the system becomes nonintegrable. It is anticipated that the ground state is still in a quasi-long-range ordered phase for a sufficiently large α, while the system favors long-range order for a small value of α. For the Heisenberg chain with staggered power-law decaying interactions, the transition between LRO phase and quasi-long-range order (QLRO) was successively investigated in literature [69–72]. At first Parreira *et al.* pointed out that the LRO is absent for $\alpha > 3$ with any λ based on spin-wave theory [69], indicating that the critical line $\alpha_c < 3$ between the AFM Néel order and the QLRO phase. Lately, Laflorencie *et al.* utilized the staggered structure factor as order parameter to detect the Néel instability in terms of quantum Monte Carlo (QMC) simulations. For $\lambda = 1$ and $\Delta^{xy} = 1$, they obtained $\alpha_c^{\mathrm{QMC}} = 2.225$, which improved the numerical results $\alpha_c^{\mathrm{SW}} = 2.46$ given by the lowest order spin-wave approximation [71]. Recently, Yang *et al.* studied the QPTs from the perspective of the fractionalized excitations for chains of length $L = 60$ using 400 density-matrix renormalization group (DMRG) states [72]. The development of the LRO is associated with the formation of coherent magnons that emerge from deconfined spinons in the gapless Luttinger liquid, giving rise to $\alpha_c^{\mathrm{DMRG}} \approx 2.2$. Thus, it would be interesting to identify the accurate value of the critical point across this unconventional phase transition by other observables with enhanced sensitivity.

As a quantum information metric, the FS has proved to be particularly useful for detecting the critical points of symmetry-knowledge unknown systems [73–75]. For a general many-body Hamiltonian $H(g)$, the ground-state FS per site can be calculated by [53,54]

$$\chi(g) = \lim_{\delta g \to 0} \frac{-2\ln F(g, \delta g)}{L(\delta g)^2}, \tag{3}$$

where the fidelity F measures the similarity between the two closest ground states $|\psi_0(g)\rangle$ and $|\psi_0(g + \delta g)\rangle$, which is defined as

$$F(g, \delta g) = |\langle \psi_0(g) | \psi_0(g + \delta g)\rangle|. \tag{4}$$

Here g is the variational parameter of $H(g)$ and δg denotes an infinitesimal deviation. Note that Hamiltonian Eq. (1) cannot be expressed as a simple form as $H(\alpha) = H_0 + \alpha H_I$. Subsequently, we obtain the derivatives of Eq. (2) as $\delta\lambda_{i,i+r} = -\lambda(-1)^r r^{-\alpha} \ln r \delta\alpha$. Due to nonfrustrated characteristics, the average derivatives of interactions per site is practically considered as an effective tuning parameter $\delta\bar{\alpha} = \sum_{i<j} \delta\lambda_{i,j}/L$.

Therefore, the FS per site can be calculated numerically by

$$\chi(\alpha) = \lim_{\delta\alpha\to 0} \frac{-2\ln F(\alpha, \delta\alpha)}{L(\delta\bar{\alpha})^2}. \tag{5}$$

The peak of FS per site is thus used to identify the phase boundary α_c for continuously varying parameters $\{\lambda, \Delta^{xy}\}$, which provides a vital opportunity to testify theoretical predictions with experimentally accessible results. Another familiar probe to monitor critical point is the bipartite von Neumann EE, which is defined by

$$S_A = -\mathrm{Tr}(\rho_A \ln \rho_A). \tag{6}$$

Here ρ_A is the reduced density matrix of subsystem A with respect to the whole system. The EE can also be extracted from the ground-state wave function $|\psi_0\rangle$ and hence properly characterize the QPTs. The ground states of short-ranged Hamiltonians usually satisfy an area law according to which the EE S_A of a subregion A of the system is proportional to the size of its boundary area. This area-law conjecture is be derived from the power-law decay of the bipartite correlations [76] and numerically verified in various quantum many-body systems, and is expected to be true in all noncritical phases [51], even for long-range interacting systems [77]. However, a logarithmic violation of the area law is usually known to occur in critical ground states, as is coined by conformal field theory (CFT), where the system size L is related to the correlation length ξ near the critical point such as $L \sim \xi$ and the gap decays as $1/L$. In this case, a coefficient proportional to the central charge of the underlying CFT, the half-chain EE of 1D critical systems of finite size L with open boundary condition satisfy

$$S_{\mathrm{h}}(L) = \frac{c}{6} \ln L + S_0, \tag{7}$$

where c is the central charge, and S_0 is a nonuniversal constant. However, the area law for long-range interacting systems is still elusive. The conformal symmetry will break down under the long-range interactions when α is small [50,78,79], as the long-range interactions results in correlation patterns similar to those in critical phases. To this end, we calculate the effective central charge c_{eff} as a function of α, which is obtained by calculating the half-chain EE for two chains with different L_1 and L_2. By using finite-size DMRG algorithm, the effective central charge can be obtained by

$$c_{\mathrm{eff}} = \frac{6[S_{\mathrm{h}}(L_2) - S_{\mathrm{h}}(L_1)]}{\ln(L_2) - \ln(L_1)}. \tag{8}$$

We emphasize that c_{eff} may not have the meaning of the central charge for the short-range interacting cases with conformal symmetries, although we find the half-chain EE always obeys the scaling form in Eq. (7).

A precise numerical determination of α_c poses significant technical challenges in terms of various criticality measures. Theoretically, the treatment of quantum many-body systems is notoriously complicated so that many investigations are still accessible by numerical techniques like the DMRG method [80–82], the present studies of Hamiltonian Eq. (1) can be simulated with very high accuracy. Based on matrix product states, we adopt both infinite-size DMRG (iDMRG) [83] and finite-size DMRG [84] where up to $m = 2000$ in the truncation of bases are kept, and this allows the truncation error to be smaller than 10^{-9}. The long-range interactions can be approximated by a summation of finite exponential terms [85,86], which inevitably introduces additional systematic error and corrupts the numerical results of FS. In our calculations of finite-size DMRG algorithm, we handle with the long-range interactions using a summation over matrix product operators (MPOs). Our codes are mainly based on iTensor C++ library [87]. Since the z-component of the total spins for the present system commutes with the Hamiltonian Eq. (1), the ground-state energy is obtained by comparing the lowest energies for each subspace of $S^z_{\mathrm{tot}} = \sum_{i=1}^{L} \langle S^z_i \rangle$. The ground state resides in the sector $S^z_{\mathrm{tot}} = 0$ as a consequence of the continuous U(1) symmetry therein.

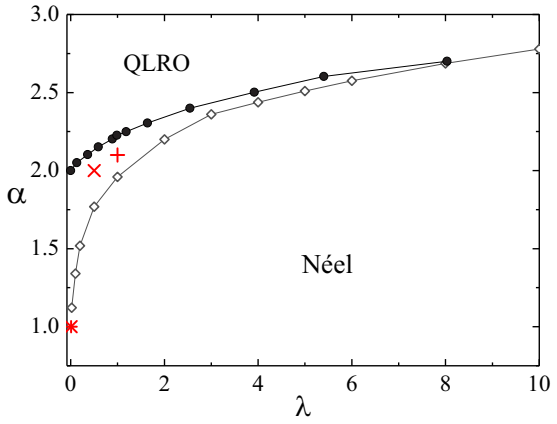

FIG. 1. Phase diagram of Hamiltonian Eq. (1) as functions of α and λ with $\Delta^{xy} = 1$. The boundary (-●-) between QLRO and LRO is computed by the large scale QMC simulation [71], and the results (-◇-) is obtained by the FS. It is noted that the LRO phase is equivalent to Néel phase in 1D spin systems. The symbols ($*$, $\times$, $+$) mark the positions of parameters used in Fig. 2.

III. RESULTS

With the DMRG algorithm at hand, we analyze the kaleidoscope of quantum phases that emerge in this system for different types of long-range exchange interactions. In the following, we will consider isotropic ($\Delta^{xy} = 1$), Ising-type ($\Delta^{xy} = 0$), and XY-type ($\Delta^{xy} = 1.5$) anisotropic cases, respectively. Using the powerful tools, the phases of long-range interacting systems are numerically diagnosed and the corresponding phase diagrams are determined.

A. $\Delta^{xy} = 1$

For the long-range isotropic Heisenberg interactions, i.e., $\Delta^{xy} = 1$, by using a combination of QMC and analytic methods, Laflorencie *et al.* have studied the phase diagram in the $\lambda - \alpha$ plane [71], as is shown in Fig. 1. It is shown that the critical point between the Néel phase and the QLRO phase increases sharply from $\alpha^c(\lambda = 0^+) = 2$ to $\alpha^c(\lambda = 8) \approx 2.7$. To further understand two phases, we investigate the correlation functions of the system using iDMRG, which can avoid the boundary effects. The correlation functions $\langle S^z_i S^z_{i+r} \rangle$ and $\langle S^+_i S^-_{i+r} \rangle$ with respect to the distance r for $\alpha = 2.1$, $\lambda = 1$ are

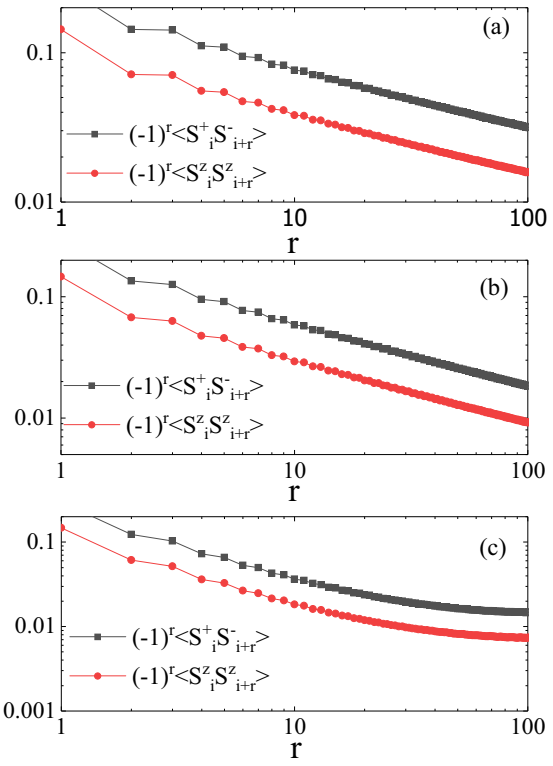

FIG. 2. Loglog-plot correlations $\langle S_i^+ S_{i+r}^- \rangle$, $\langle S_i^z S_{i+r}^z \rangle$ versus the distance r with $\Delta^{xy} = 1$ for (a) $\lambda = 1$, $\alpha = 2.10$; (b) $\lambda = 0.5$, $\alpha = 2$ and (c) $\lambda = 0.01$, $\alpha = 1$.

shown in Fig. 2(a). As we know, for 1D spin-1/2 short-range AFM Heisenberg system, the spin-spin correlation function

$$\langle \vec{S}_i \cdot \vec{S}_{i+r} \rangle \propto \frac{(-1)^r \sqrt{\ln r}}{r}, \tag{9}$$

is expected to characterize the QLRO phase, and

$$\lim_{r \to +\infty} \langle \vec{S}_i \cdot \vec{S}_{i+r} \rangle = \pm m_c^2 \tag{10}$$

is capable of identifying the Néel phase [88]. The power-law decay of $\langle S_i^z S_{i+r}^z \rangle$, $\langle S_i^+ S_{i+r}^- \rangle$ in Fig. 2(a), implies $\lim_{r\to\infty} \langle \vec{S}_i \cdot \vec{S}_{i+r} \rangle$ would approach zero and the ground state for $\{\alpha = 2.1, \lambda = 1\}$ under consideration is within the QLRO phase and thus the critical point of Néel-to-QLRO transition should be below 2.1 for $\lambda = 1$. The spatial correlation functions for $\{\alpha = 2, \lambda = 0.5\}$ are also calculated, and the QMC results showcase the system should be in Néel phase. One finds $\langle S_i^z S_{i+r}^z \rangle$ and $\langle S_i^+ S_{i+r}^- \rangle$ also exhibit a power-law decay, as is observed in Fig. 2(b), which means the ground state remains the QLRO phase. These above mentioned discoveries indicate the critical points retrieved by the QMC are not accurate. A more creditable measure should be adopted to determine the phase boundaries.

To alleviate the controversy by the discrepancy between the QMC results (cf. Fig. 1) and correlations (cf. Fig. 2), we consider a limiting case, i.e., $\lambda \to \infty$, which can be equivalently implemented by switching off the nearest-neighbor isotropic interactions in Hamiltonian Eq. (1) with finite λ. The absence of the LRO has been rigorously proven for $\alpha > 3$ with $\lambda = 1$ [69,89], and was lately extended to arbitrary λ

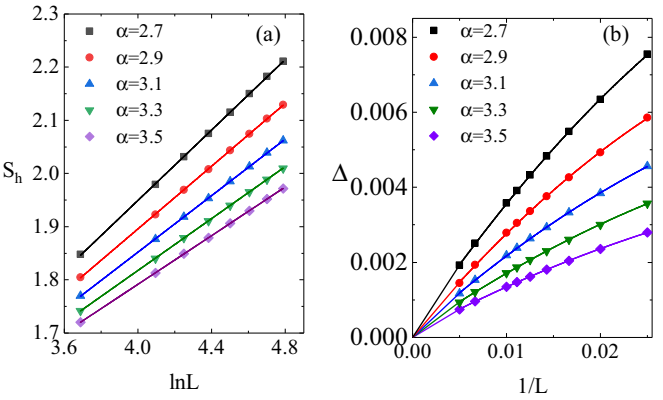

FIG. 3. (a) Half-chain EE versus $\ln L$ for different α with Δ^{xy}=1, $\lambda = \infty$. Symbols show numerical results obtained by DMRG calculations, and solid lines are linear fits of the data. (b) Finite-size scaling of the energy gap Δ with various α. Symbols show numerical results obtained by DMRG calculations, and solid lines are fits of the data by quadratic polynomials in $1/L$.

[71]. The critical point $\alpha_c^{\rm SW}(\lambda \to \infty) = 2.9032$ was inferred by the spin-wave approximation [71]. In this case, we use the EE to speculate the critical point. We find the EE decreases monotonically with increasing α. In particular, the EE always shows a logarithmic growth with the system size as $S_{\rm h} \propto \ln L$ [Fig. 3(a)], which can be treated as reminiscent of gapless ground state in both the QLRO phase and the Néel phase [72], as is indicated in Fig. 3(b). Consequently the signal of the QPT is hardly discerned from the EE.

The impetus to identify the precise position of the quantum critical point(QCP) was given by the FS, which has been proven to be capable of detecting the phase transition successfully between two gapless phases [49]. To this end, we will adopt the FS to identify the QCP between the Néel phase with LRO and the QLRO phase for $\lambda = \infty$ as a glimpse. The numerical results are shown in Fig. 4(a). One can observe the peak of the FS increases with the system size L nearby $\alpha = 3.1$. To locate the critical points α_c in the thermodynamic limit, we have used the finite-size scaling theory [90], which

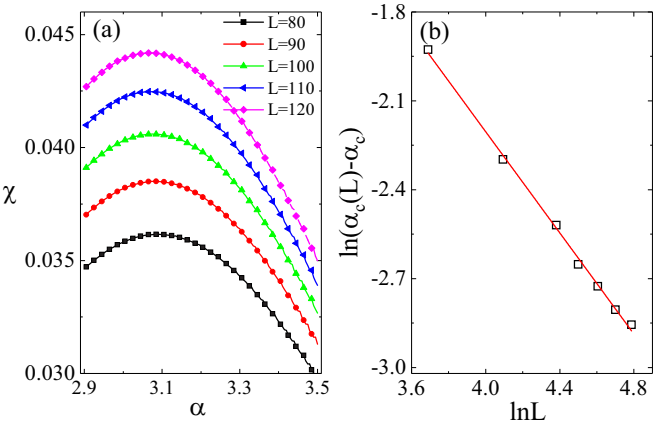

FIG. 4. (a) Fidelity susceptibility per site is plotted as a function of the parameter α on different system sizes L with $\Delta^{xy} = 1$, $\lambda = \infty$. (b) Scaling of the peak positions of χ.

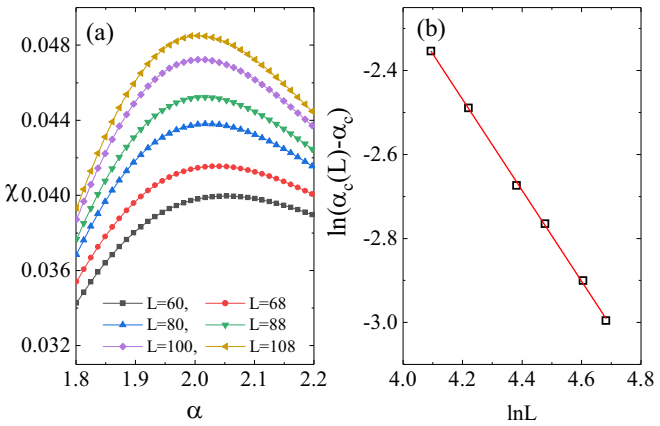

FIG. 5. (a) Fidelity susceptibility per site is plotted as a function of the parameter α on different system sizes L with $\Delta^{xy} = 1$, $\lambda = 1$. (b) The corresponding scaling of the peak positions of χ.

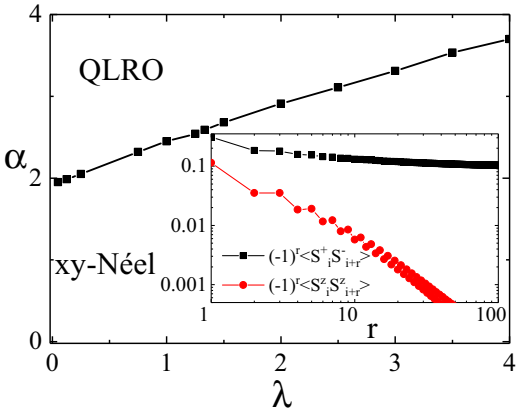

FIG. 6. Phase diagram of Hamiltonian Eq. (1) as functions of α and λ with $\Delta^{xy} = 1.5$. Inset: Correlations $\langle S_i^+ S_{i+r}^- \rangle$, $\langle S_i^z S_{i+r}^z \rangle$ versus the distance r for $\lambda = 1$, $\alpha = 2$ with $\Delta^{xy} = 1.5$.

can be used in finite systems with long-range interactions [91]. The position of the maximal points of the FS can be fitted by the following formula:

$$|\alpha_c(L) - \alpha_c| \sim L^{-b}, \tag{11}$$

where b is a constant and α_c is the QCP in the thermodynamic limit. For properly chosen values of $\alpha_c = 3.00$, $b = 0.85$, we can see from Fig. 4(b) that a linear relation following Eq. (11) for different L is verified. Our results indicate the critical points α_c would approach 3.0 as $\lambda \to \infty$. Recall that Parreira *et al.* pointed out the nonexistence of the Néel phase at zero temperature for $\alpha > 3$ for $\lambda = 1$ [69] and a straightforward extension for all λ [71]. In this sense, the surprising consistence between our result with the previous results confirm that the FS shows high accuracy and reliability in detecting the critical point of the Néel-to-QLRO transitions.

Next we investigate the case of $\lambda = 1$. The FS results for various system sizes are shown in Fig. 5(a). The corresponding finite-size scaling according to Eq. (11) is illustrated in Fig. 5(b), giving rise to $\alpha_c = 1.955$, $b = 1.0$. In contrast to the QMC result $\alpha_c^{\mathrm{QMC}} = 2.225 \pm 0.025$ and the spin-wave result $\alpha_c^{\mathrm{SW}} = 2.46$, the obtained value of α_c indicates that the ground state for $\alpha = 2.1$ is within the QLRO phase. This is consistent with the correlations in Fig. 2(a). To this end, the FS is calculated for different λ and the positions of critical points can be precisely retrieved from the FS results for $\lambda \geqslant 0.02$. One finds $\alpha_c \simeq 1.12$ for $\lambda = 0.02$, whereas the positions of the critical points become elusive through the peak of the FS for $\lambda < 0.02$. As is observed in Fig. 2(c), it is found that the correlations $\langle S_i^z S_{i+r}^z \rangle$, $\langle S_i^+ S_{i+r}^- \rangle$ tend to a constant for $\{\alpha = 1, \lambda = 0.01\}$, implying that the critical point $\alpha_c \geqslant 1$ when $\lambda \to 0^+$, which is consistent with spin-wave result. Based on the above analysis of correlation functions and the FS, we obtain the critical points and establish the ground-state phase diagram in Fig. 1. It is clear that the critical values $a_c(\lambda)$ get lower than those obtained by the large scale QMC simulation. The deviation is extremely prominent for small λ but negligible for large λ.

B. $\Delta^{xy} = 1.5$

Next, we begin to study the effect of anisotropy of long-range exchange interactions. First, the XY-type ($\Delta^{xy} > 1$) exchange interactions are considered. The phase diagram of Hamiltonian Eq. (1) with $\Delta^{xy} = 1.5$ as functions of α and λ is shown in Fig. 6. For sufficiently large α, the system would be in the QLRO phase. As the decay exponent α gets smaller, the long-range interactions will become dominated. The correlation functions for $\{\alpha = 2, \lambda = 1\}$ are shown in the inset of Fig. 6, where $\langle S_i^z S_{i+r}^z \rangle$ tends to vanish as $r \to \infty$, while $\langle S_i^+ S_{i+r}^- \rangle$ will alternate between -0.1 and 0.1, which means that the xy-Néel phase is stabilized with breaking of the continuous U(1) symmetry in the x-y plane. In a sense, the correlation function $\langle S_i^+ S_{i+r}^- \rangle$ can act as an order parameter for the QPT between the QLRO and U(1)-symmetric broken phase. The ground-state FS per site χ for $\lambda = 1$ is exhibited in Fig. 7(a). Following the similar strategy as SU(2) symmetric model, the critical point $\alpha_c = 2.42$ between the xy-Néel and QLRO phase is identified from Fig. 7(b). Similarly, the EE scales logarithmically with the system size in the xy-Néel

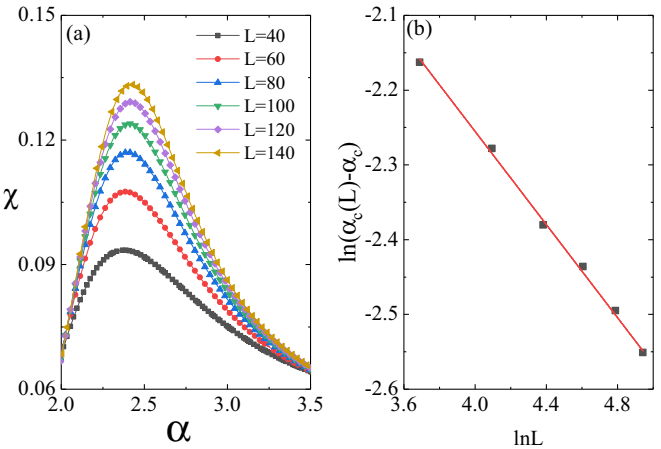

FIG. 7. (a) Fidelity susceptibility per site is plotted as a function of the parameter α on different system sizes L with $\lambda = 1$, $\Delta^{xy} = 1.5$. (b) The corresponding scaling of the peak positions of χ.

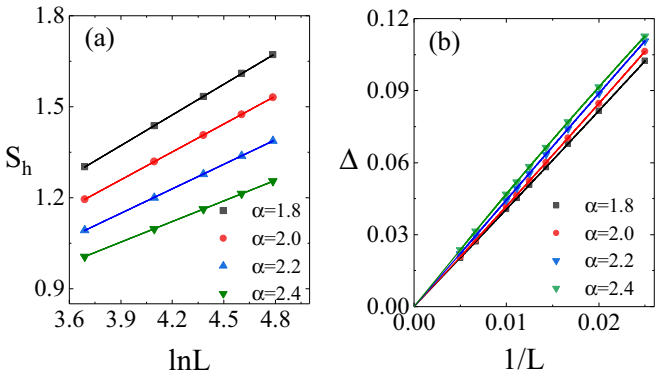

FIG. 8. (a) Half-chain EE versus $\ln L$ for different α with $\Delta^{xy} = 1.5$, $\lambda = 1$. (b) Finite-size scaling of the energy gap Δ with various α. Symbols show numerical results obtained by DMRG calculations, and solid lines are linear fits of the data in $1/L$.

phase, as is disclosed in Fig. 8(a), suggesting that the xy-Néel phase remains gapless. To validate the gapless nature, the finite-size energy gap $\Delta(L)$ is calculated for $\alpha < \alpha_c$ in Fig. 8(b). The linear fitting with respect to $1/L$ designates that $\Delta(\infty)$ will vanish in the thermodynamic limit and the dynamical exponent $z = 1$.

C. $\Delta^{xy} = 0$

We can consider the Ising-type ($\Delta^{xy} < 1$) long-range interactions. Here we exhibit a special case, i.e., $\Delta^{xy} = 0$. The phase diagram of Hamiltonian Eq. (1) as functions of α and λ is shown in Fig. 9. For sufficiently large α, the system also would enter the QLRO phase. As the decay exponent α decreases, the long-range Ising interactions will become dominated. The correlation functions for $\{\alpha = 3, \lambda = 1\}$ are shown in the inset of Fig. 9, where $\langle S_i^+ S_{i+r}^-\rangle$ exhibits an oscillating decay until vanishes as $r \to \infty$, while $\langle S_i^z S_{i+r}^z\rangle$ alternates between -0.053 and 0.053, implying the characteristic of $\mathbb{Z}_2$ symmetry broken z-Néel phase.

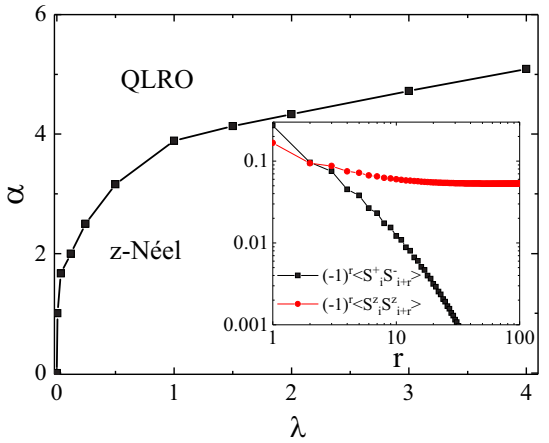

FIG. 9. (a) Phase diagram of Hamiltonian Eq. (1) as functions of α and λ with $\Delta^{xy} = 0$. Inset: Correlations $\langle S_i^+ S_{i+r}^-\rangle$, $\langle S_i^z S_{i+r}^z\rangle$ versus the distance r for $\lambda = 1$, $\alpha = 3$ with $\Delta^{xy} = 0$.

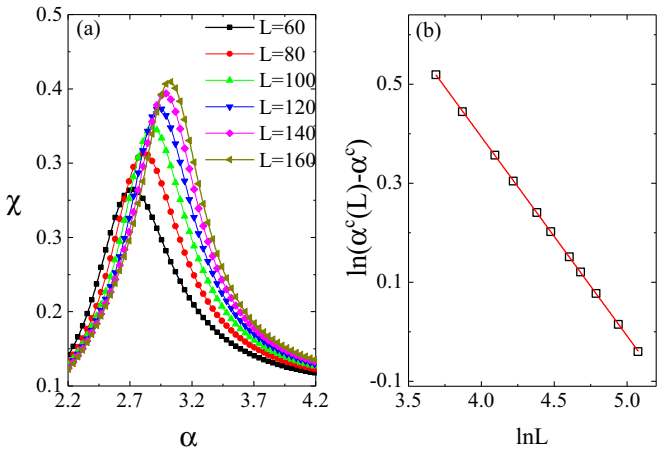

FIG. 10. (a) Fidelity susceptibility per site is plotted as a function of the parameter α on different system sizes L with $\Delta^{xy} = 0$, $\lambda = 1$. (b) The corresponding scaling of the peak positions of χ.

Moreover, we find that the phase transitions between z-Néel and QLRO can be sensitively detected by both the FS and the EE. In Fig. 10(a), the FS per site with respect to α for different system sizes L is presented and the peak of the ground-state FS becomes pronounced with increasing system sizes, which signals the occurrence of the QPT. Regarding the finite-size scaling in Eq. (11), $\alpha_c = 3.88$ and $b = 0.40$ can be extracted from Fig. 10(b). Further evidence for indicating the z-Néel-to-QLRO transition is provided by the EE, which is shown in Fig. 11(a). Upon increasing the system size L, the EE shows a logarithmic growth for $\alpha > \alpha_c$ but saturates

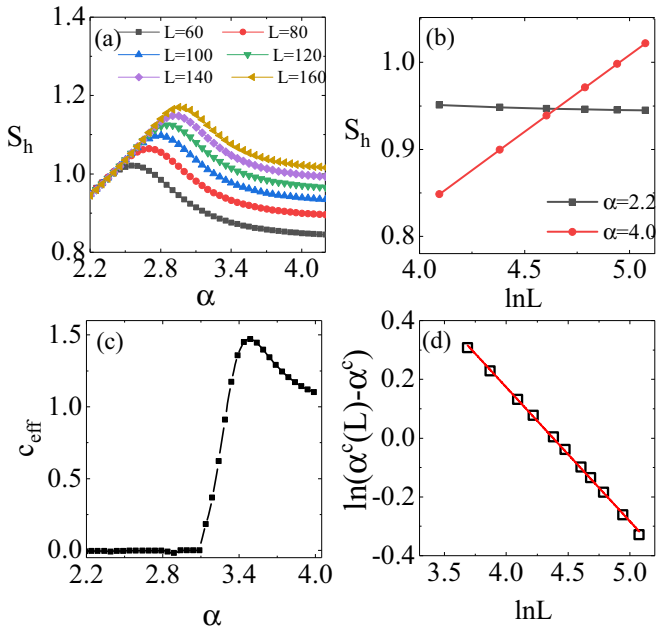

FIG. 11. (a) Half-chain EE is plotted as a function of the decay exponent α on different system sizes L with $\Delta^{xy} = 0$, $\lambda = 1$. (b) Half-chain EE versus $\ln L$ for different α. (c) The effective central charge in Eq. (8), versus α with $L_1 = 400$ and $L_2 = 500$. (d) The corresponding scaling of peak positions of S_h.

quickly otherwise [see Fig. 11(b)], suggesting the z-Néel phase is gapped and the breaking of conformal symmetry. The effective central charge c_{eff} would be zero [cf. Fig. 11(c)]. Similar to that of the FS, the finite-size scaling of the EE yields $\alpha_c = 3.88$, $b = 0.457$, as is exhibited in Fig. 11(d). It is worthy noting that the critical point α_c with $\Delta^{xy} = 0$ becomes vanishing when the parameter λ tends to zero, and diverges when λ increases to the infinity.

IV. DISCUSSION

In this paper, we have studied the quantum phase transitions (QPTs) in the one-dimensional spin-1/2 chains with modulated long-range power-law-decaying interactions in terms of the density-matrix renormalization group technique. Together with the correlations and the entanglement entropy (EE), the ground-state fidelity susceptibility (FS) are employed to determine the phase boundary. The XY-type long-range interactions lead to the emergence of U(1)-symmetric broken xy-Néel phase with long-range order (LRO) along easy axes [92], akin to the SU(2) symmetry broken Néel phase induced by isotropic long-range interactions, while the Ising-type long-range interactions prompt the $\mathbb{Z}_2$ symmetry broken z-Néel phase. The FS can detect the QPT between the gapless quasi-long-range order (QLRO) phase and three different Néel phase, whether it is gapless or not. The FS proved to be a reliable tool to determine the ground-state phase diagram. An area-law scaling is still valid in the gapped phase in the presence of the long-range interactions, although it was originally derived for the short-range interacting Hamiltonian. Figures 3(a) and 8(a) demonstrate that the half-chain EE satisfies a logarithmic scaling with respect to the system size in gapless phases. In this respect, the half-chain EE can faithfully seize the QPT between the gapless QLRO phase and the gapped z-Néel phase, while it is insensitive to QPTs between two gapless phases, such as QLRO to xy-Néel phase transition, QLRO to Néel phase transition. The insensitivity of the EE at quantum critical points between gapless phases may be traced back to the gapless mode associated with the spontaneous breaking of the continuous symmetry, sparking the challenge to demand much larger-scale computation for the effective central charge. In this context, using the maximum of bipartite EE as an indicator of a QPT from a gapless phase to another gapless phase is still elusive. The models under consideration could be envisioned in quantum simulation in ultracold atoms [67,93], opening the prospect for experimental investigation of the issues confronted here.

ACKNOWLEDGMENTS

W.-L.Y. appreciates the valuable discussion with Gaoyong Sun and Ming Xue. This work is supported by the National Natural Science Foundation of China (NSFC) under Grants No. 11104021 and No. 12174194. J.R. kindly acknowledges support from Open Project of Key Laboratory of Artificial Structures and Quantum Control (Ministry of Education), Shanghai Jiao Tong University. W.-L.Y. acknowledges the startup fund of Nanjing University of Aeronautics and Astronautics under Grant No. 1008-YAH20006, Top-notch Academic Programs Project of Jiangsu Higher Education Institutions and stable supports for basic institute research (Grant No. 190101).

[1] A. Auerbach, *Interacting Electrons and Quantum Magnetism* (Springer-Verlag, New York, NY, 1994).

[2] S. Chen, L. Wang, S.-J. Gu, and Y. Wang, Fidelity and quantum phase transition for the Heisenberg chain with next-nearest-neighbor interaction, Phys. Rev. E **76**, 061108 (2007).

[3] T.-C. Yi, W.-L. You, N. Wu, and A. M. Oleś, Criticality and factorization in the Heisenberg chain with Dzyaloshinskii-Moriya interaction, Phys. Rev. B **100**, 024423 (2019).

[4] W.-L. You, P. Horsch, and A. M. Oleś, Quantum phase transitions in exactly solvable one-dimensional compass models, Phys. Rev. B **89**, 104425 (2014).

[5] W.-L. You, G. Sun, J. Ren, W. C. Yu, and A. M. Oleś, Quantum phase transitions in the spin-1 Kitaev-Heisenberg chain, Phys. Rev. B **102**, 144437 (2020).

[6] W.-L. You, Z. Zhao, J. Ren, G. Sun, L. Li, and A. M. Oleś, Quantum many-body scars in spin-1 Kitaev chains, Phys. Rev. Research **4**, 013103 (2022).

[7] D. C. Mattis, *The Theory of Magnetism Made Simple: An Introduction to Physical Concepts and to Some Useful Mathematical Methods* (World Scientific, Singapore, 2006).

[8] M. Žnidaric, T. Prosen, and P. Prelovšek, Many-body localization in Heisenberg XXZ magnet in a random field, Phys. Rev. B **77**, 064426 (2008).

[9] J.-W. Mei, J.-Y. Chen, H. He, and X.-G. Wen, Gapped spin liquid with Z_2-topological order for kagome Heisenberg model, Phys. Rev. B **95**, 235107 (2017).

[10] Y. A. Kharkov, V. E. Sotskov, A. A. Karazeev, E. O. Kiktenko, and A. K. Fedorov, Revealing quantum chaos with machine learning, Phys. Rev. B **101**, 064406 (2020).

[11] M. A. Nielsen and I. L. Chuang, *Quantum Computation and Quantum Information* (Cambridge University Press, Cambridge, UK, 2000).

[12] W.-L. You, Long-range order in two-dimensional XXZ model, Int. J. Mod. Phys. B **23**, 2195 (2009).

[13] S. Tang and J. E. Hirsch, Long-range order without broken symmetry: Two-dimensional Heisenberg antiferromagnet at zero temperature, Phys. Rev. B **39**, 4548 (1989).

[14] H. Q. Lin and D. K. Campbell, Long-Range Order in the 2D Antiferromagnetic Heisenberg Model: A Renormalization Perspective, Phys. Rev. Lett. **69**, 2415 (1992).

[15] F. D. M. Haldane, Continuum dynamics of the 1-D Heisenberg antiferromagnetic identification with the O(3) nonlinear sigma model, Phys. Lett. A **93**, 464 (1983).

[16] F. D. M. Haldane, Nonlinear Field Theory of Large-Spin Heisenberg Antiferromagnets: Semiclassically Quantized Solitons of the One-Dimensional Easy-Axis Néel State, Phys. Rev. Lett. **50**, 1153 (1983).

[17] P. R. Hammar, M. B. Stone, Daniel H. Reich, C. Broholm, P. J. Gibson, M. M. Turnbull, C. P. Landee, and M. Oshikawa, Characterization of a quasi-one-dimensional spin-1/2 magnet which is gapless and paramagnetic for $g\mu_B H \lesssim J$ and $k_B T \ll J$, Phys. Rev. B **59**, 1008 (1999).

[18] M. D. Johannes, J. Richter, S.-L. Drechsler, and H. Rosner, $Sr_2Cu(PO_4)_2$: A real material realization of the one-dimensional nearest-neighbor Heisenberg chain, Phys. Rev. B **74**, 174435 (2006).

[19] B. Lake, D. A. Tennant, J.-S. Caux, T. Barthel, U. Schollwöck, S. E. Nagler, and C. D. Frost, Multispinon Continua at Zero and Finite Temperature in a Near-Ideal Heisenberg Chain, Phys. Rev. Lett. **111**, 137205 (2013).

[20] M. Mourigal, M. Enderle, A. Klöpperpieper, J.-S. Caux, A. Stunault, and H. M. Rønnow, Fractional spinon excitations in the quantum Heisenberg antiferromagnetic chain, Nat. Phys. **9**, 435 (2013).

[21] A. K. Bera, B. Lake, A. T. M. N. Islam, B. Klemke, E. Faulhaber, and J. M. Law, Field-induced magnetic ordering and single-ion anisotropy in the quasi-one-dimensional Haldane chain compound $SrNi_2V_2O_8$: A single-crystal investigation, Phys. Rev. B **87**, 224423 (2013).

[22] A. K. Bera, B. Lake, A. T. M. N. Islam, O. Janson, H. Rosner, A. Schneidewind, J. T. Park, E. Wheeler, and S. Zander, Consequences of critical interchain couplings and anisotropy on a Haldane chain, Phys. Rev. B **91**, 144414 (2015).

[23] T. Delica, K. Kopinga, H. Leschke, and K. K. Mon, Thermal properties of chains of antiferromagnetically coupled spins with $s = 1$. Numerical evidence of the Haldane gap at nonzero temperatures, Europhys. Lett. **15**, 55 (1991).

[24] O. Avenel, J. Xu, J. S. Xia *et al.*, Low-temperature magnetic measurements of an $S = 1$ linear-chain Heisenberg antiferromagnet, Phys. Rev. B **46**, 8655(R) (1992).

[25] R. C. Williams, W. J. A. Blackmore, S. P. M. Curley, M. R. Lees, S. M. Birnbaum, J. Singleton, B. M. Huddart, T. J. Hicken, T. Lancaster, S. J. Blundell, F. Xiao, A. Ozarowski, F. L. Pratt, D. J. Voneshen, Z. Guguchia, C. Baines, J. A. Schlueter, D. Y. Villa, J. L. Manson, and P. A. Goddard, Near-ideal molecule-based Haldane spin chain, Phys. Rev. Research **2**, 013082 (2020).

[26] N. Defenu, T. Donner, T. MacrMacrì, G. Pagano, S. Ruffo, and A. Trombettoni, Long-range interacting quantum systems, arXiv:2109.01063.

[27] J. C. Tung and G. Y. Guo, *Ab initio* studies of spin-spiral waves and exchange interactions in 3D transition metal atomic chains, Phys. Rev. B **83**, 144403 (2011).

[28] S. T. Bramwell and M. J. P. Gingras, Spin ice state in frustrated magnetic pyrochlore materials, Science **294**, 1495 (2001).

[29] C. Castelnovo, R. Moessner, and S. L. Sondhi, Magnetic monopoles in spin ice, Nature (London) **451**, 42 (2008).

[30] A. M. Black-Schaffer, RKKY coupling in graphene, Phys. Rev. B **81**, 205416 (2010).

[31] I. Bloch, J. Dalibard, and W. Zwerger, Many-body physics with ultracold gases, Rev. Mod. Phys. **80**, 885 (2008).

[32] I. Bloch, J. Dalibard, and S. Nascimbene, Quantum simulations with ultracold quantum gases, Nat. Phys. **8**, 267 (2012).

[33] K. Kim, M. S. Chang, S. Korenblit, R. Islam, E. E. Edwards, J. K. Freericks, G. D. Lin, L. M. Duan, and C. Monroe, Quantum simulation of frustrated Ising spins with trapped ions, Nature (London) **465**, 590 (2010).

[34] C. Senko, P. Richerme, J. Smith, A. Lee, I. Cohen, A. Retzker, and C. Monroe, Realization of a Quantum Integer-Spin Chain with Controllable Interactions, Phys. Rev. X **5**, 021026 (2015).

[35] H. Ritsch, P. Domokos, F. Brennecke, and T. Esslinger, Cold atoms in cavity-generated dynamical optical potentials, Rev. Mod. Phys. **85**, 553 (2013).

[36] M. Saffman, T. G. Walker, and K. Mølmer, Quantum information with Rydberg atoms, Rev. Mod. Phys. **82**, 2313 (2010).

[37] E. Guardado-Sanchez, P. T. Brown, D. Mitra, T. Devakul, D. A. Huse, P. Schauß, and W. S. Bakr, Probing the quench dynamics of antiferromagnetic correlations in a 2D quantum Ising spin system, Phys. Rev. X **8**, 021069 (2018).

[38] S. de Léséleuc, V. Lienhard, P. Scholl, D. Barredo, S. Weber, N. Lang, H. P. Büchler, T. Lahaye, and A. Browaeys, Observation of a symmetry-protected topological phase of interacting bosons with Rydberg atoms, Science **365**, 775 (2019).

[39] A. W. Glaetzle, M. Dalmonte, R. Nath, C. Gross, I. Bloch, and P. Zoller, Designing Frustrated Quantum Magnets with Laser-Dressed Rydberg Atoms, Phys. Rev. Lett. **114**, 173002 (2015).

[40] I. Bouchoule and K. Mølmer, Spin squeezing of atoms by the dipole interaction in virtually excited Rydberg states, Phys. Rev. A **65**, 041803(R) (2002).

[41] G. Pupillo, A. Micheli, M. Boninsegni, I. Lesanovsky, and P. Zoller, Strongly Correlated Gases of Rydberg-Dressed Atoms: Quantum and Classical Dynamics, Phys. Rev. Lett. **104**, 223002 (2010).

[42] N. Henkel, R. Nath, and T. Pohl, Three-Dimensional Roton Excitations and Supersolid Formation in Rydberg-Excited Bose-Einstein Condensates, Phys. Rev. Lett. **104**, 195302 (2010).

[43] W. Li, L. Hamadeh, and I. Lesanovsky, Probing the interaction between Rydberg-dressed atoms through interference, Phys. Rev. A **85**, 053615 (2012).

[44] A. Isidori, A. Ruppel, A. Kreisel, P. Kopietz, A. Mai, and R. M. Noack, Quantum criticality of dipolar spin chains, Phys. Rev. B **84**, 184417 (2011).

[45] F. D. M. Haldane, Exact Jastrow-Gutzwiller Resonating-Valence-Bond Ground State of the Spin-1/2 Antiferromagnetic Heisenberg Chain with $1/r^2$ Exchange, Phys. Rev. Lett. **60**, 635 (1988).

[46] Z. X. Gong, M. F. Maghrebi, A. Hu, M. L. Wall, M. Foss-Feig, and A. V. Gorshkov, Topological phases with long-range interactions, Phys. Rev. B **93**, 041102(R) (2016).

[47] Z. X. Gong, M. F. Maghrebi, A. Hu, M. Foss-Feig, P. Richerme, C. Monroe, and A. V. Gorshkov, Kaleidoscope of quantum phases in a long-range interacting spin-1 chain, Phys. Rev. B **93**, 205115 (2016).

[48] Z. H. Li, Ground states of long-range interacting fermions in one spatial dimension, J. Phys.: Condens. Matter **31**, 255601 (2019).

[49] J. Ren, W. L. You, and X. Wang, Entanglement and correlations in a one-dimensional quantum spin-$\frac{1}{2}$ chain with anisotropic power-law long-range interactions, Phys. Rev. B **101**, 094410 (2020).

[50] M. F. Maghrebi, Z. X. Gong, and A. V. Gorshkov, Continuous Symmetry Breaking in 1D Long-Range Interacting Quantum Systems, Phys. Rev. Lett. **119**, 023001 (2017).

[51] L. Amico, R. Fazio, A. Osterloh, and V. Vedral, Entanglement in many-body systems, Rev. Mod. Phys. **80**, 517 (2008).

[52] N. Laflorencie, Quantum entanglement in condensed matter systems, Phys. Rep. **646**, 1-59 (2016).
[53] S.-J. Gu, Fidelity approach to quantum phase transitions, Int. J. Mod. Phys. B **24**, 4371 (2010), and more references therein.
[54] W. L. You, Y. W. Li, and S. J. Gu, Fidelity, dynamic structure factor, and susceptibility in critical phenomena, Phys. Rev. E **76**, 022101 (2007).
[55] T. J. Osborne and M. A. Nielsen, Entanglement in a simple quantum phase transition, Phys. Rev. A **66**, 032110 (2002).
[56] J. Ren, G. H. Liu, and W. L. You, Entanglement entropy and fidelity susceptibility in the one-dimensional spin-1 XXZ chains with alternating single-site anisotropy, J. Phys.: Condens. Matter **27**, 105602 (2015).
[57] J. Ren, Y. M. Wang, and W. L. You, Quantum phase transitions in spin-1 XXZ chains with rhombic single-ion anisotropy, Phys. Rev. A **97**, 042318 (2018).
[58] G. Sun, A. K. Kolezhuk, and T. Vekua, Fidelity at Berezinskii-Kosterlitz-Thouless quantum phase transitions, Phys. Rev. B **91**, 014418 (2015).
[59] B. Wang, M. Feng, and Z. Q. Chen, Berezinskii-Kosterlitz-Thouless transition uncovered by the fidelity susceptibility in the XXZ model, Phys. Rev. A **81**, 064301 (2010).
[60] Q. Luo, J. Zhao, and X. Wang, Fidelity susceptibility of the anisotropic XY model: The exact solution, Phys. Rev. E **98**, 022106 (2018).
[61] T. Lv, T.-C. Yi, L. Li, G. Sun, and W.-L. You, Quantum criticality and universality in the p-wave-paired Aubry-André-Harper model, Phys. Rev. A **105**, 013315 (2022).
[62] J. Ren, W.-L. You, and A. M. Oleś, Quantum phase transitions in a spin-1 antiferromagnetic chain with long-range interactions and modulated single-ion anisotropy, Phys. Rev. B **102**, 024425 (2020).
[63] G. Sun, Fidelity susceptibility study of quantum long-range antiferromagnetic Ising chain, Phys. Rev. A **96**, 043621 (2017).
[64] Z. Zhu, G. Sun, W.-L. You, and D.-N. Shi, Fidelity and criticality of a quantum Ising chain with long-range interactions, Phys. Rev. A **98**, 023607 (2018).
[65] A. Chiocchetta, D. Kiese, C. Philipp Zelle, F. Piazza, and S. Diehl, Cavity-induced quantum spin liquids, Nat. Commun. **12**, 5901 (2021).
[66] V. D. Vaidya, Y. Guo, R. M. Kroeze, K. E. Ballantine, A. J. Kollár, J. Keeling, and B. L. Lev, Tunable-range, photon-mediated atomic interactions in multimode cavity QED, Phys. Rev. X **8**, 011002 (2018).
[67] A. Periwal, E. S. Cooper, P. Kunkel, J. F. Wienand, E. J. Davis, and M. Schleier-Smith, Programmable interactions and emergent geometry in an array of atom clouds, Nature (London) **600**, 630 (2021).
[68] H. A. Bethe, On the theory of metal I. Eigenvalues and eigenfunctions of a linear chain of atoms, Z. Phys. **71**, 205 (1931).
[69] J. R. Parreira, O. Bolina, and J. F. Perez, Néel order in the ground state of Heisenberg antiferromagnetic chains with long-range interactions, J. Phys. A: Math. Gen. **30**, 1095 (1997).
[70] A. W. Sandvik, Ground States of a Frustrated Quantum Spin Chain with Long-Range Interactions, Phys. Rev. Lett. **104**, 137204 (2010).
[71] N. Laflorencie, I. Affleck, and M. Berciu, Critical phenomena and quantum phase transition in long-range Heisenberg antiferromagnetic chains, J. Stat. Mech. (2005) P12001.
[72] L. Yang and A. E. Feiguin, From deconfined spinons to coherent magnons in an antiferromagnetic Heisenberg chain with long range interactions, SciPost Phys. **10**, 110 (2021).
[73] Y. Wang, W.-L. You, M. Liu, Y.-L. Dong, H.-G. Luo, G. Romero, and J. Q. You, Quantum criticality and state engineering in the simulated anisotropic quantum Rabi model, New J. Phys. **20**, 053061 (2018).
[74] B.-B. Wei and X.-C. Lv, Fidelity susceptibility in the quantum Rabi model, Phys. Rev. A **97**, 013845 (2018).
[75] Z.-A. Liu, Y.-L. Dong, N. Wu, Y. Wang, and W.-L. You, Quantum criticality and correlations in the Ising-Gamma chain, Physica A **579**, 126122 (2021).
[76] M. B. Hastings and T. Koma, Spectral gap and exponential decay of correlations, Commun. Math. Phys. **265**, 781 (2006).
[77] T. Kuwahara and K. Saito, Area law of noncritical ground states in 1D long-range interacting systems, Nat. Commun. **11**, 4478 (2020).
[78] D. Vodola, L. Lepori, E. Ercolessi, A. V. Gorshkov, and G. Pupillo, Kitaev Chains with Long-Range Pairing, Phys. Rev. Lett. **113**, 156402 (2014).
[79] D. Vodola, L. Lepori, E. Ercolessi, and G. Pupillo, Long-range Ising and Kitaev models: Phases, correlations and edge modes, New J. Phys. **18**, 015001 (2016).
[80] S. R. White, Density-matrix algorithms for quantum renormalization groups, Phys. Rev. B **48**, 10345 (1993).
[81] I. Peschel, X. Q. Wang, M. Kaulke, and K. Hallberg, *Density Matrix Renormalization*, Lecture Notes in Physics Vol. 528 (Springer, Berlin, 1999).
[82] U. Schollwöck, The density-matrix renormalization group, Rev. Mod. Phys. **77**, 259 (2005).
[83] I. P. McCulloch, Infinite-size density-matrix renormalization group, revisited, arXiv:0804.2509.
[84] U. Schollwöck, The density-matrix renormalization group in the age of matrix product states, Ann. Phys. (NY) **326**, 96 (2011).
[85] G. M. Crosswhite, A. C. Doherty, and G. Vidal, Applying matrix product operators to model systems with long-range interactions, Phys. Rev. B **78**, 035116 (2008).
[86] B. Pirvu, V. Murg, J. I. Cirac, and F. Verstraete, Matrix product operator representations, New J. Phys. **12**, 025012 (2010).
[87] M. Fishman, S. R. White, and E. Miles Stoudenmire, The ITensor Software Library for Tensor Network, arXiv:2007.14822.
[88] I. Affleck, D. Gepner, H. J. Schulz, and T. Ziman, Critical behaviour of spin-s Heisenberg antiferromagnetic chains: Analytic and numerical results, J. Phys. A: Math. Gen. **22**, 511 (1989).
[89] I. Frénot, P. Naldesi, and T. Roscilde, Entanglement and fluctuations in the XXZ model with power-law interactions, Phys. Rev. B **95**, 245111 (2017).
[90] M. E. Fisher and M. N. Barber, Scaling Theory for Finite-Size Effects in the Critical Region, Phys. Rev. Lett. **28**, 1516 (1972).
[91] E. S. Loscar and C. M. Horowitz, Size effects in finite systems with long-range interactions, Phys. Rev. E **97**, 032103 (2018).
[92] Z. Li, S. Choudhury, and W. Vincent Liu, Long-range-ordered phase in a quantum Heisenberg chain with interactions beyond nearest neighbors, Phys. Rev. A **104**, 013303 (2021).
[93] F. Schäfer, T. Fukuhara, S. Sugawa, Y. Takasu, and Y. Takahashi, Tools for quantum simulation with ultracold atoms in optical lattices, Nat. Rev. Phys. **2**, 411 (2020), and references therein.